



Dalton
Transactions

Pressure and Temperature Dependences of the Canting Angle and Increase in the Magnetic Ordering Temperature, $T_c(P)$, for the Weak Ferromagnet $\text{Li}^+[\text{TCNE}]^{\bullet-}$ (TCNE = Tetracyanoethylene)

Journal:	<i>Dalton Transactions</i>
Manuscript ID	DT-ART-08-2021-002647.R1
Article Type:	Paper
Date Submitted by the Author:	03-Sep-2021
Complete List of Authors:	Miller, Joel; University of Utah, Department of Chemistry Davidson, Royce; University of Utah

SCHOLARONE™
Manuscripts

Pressure and Temperature Dependences of the Canting Angle and Increase in the Magnetic Ordering Temperature, $T_c(P)$, for the Weak Ferromagnet $\text{Li}^+[\text{TCNE}]^-$ (TCNE = Tetracyanoethylene)

Royce A. Davidson, Joel S. Miller*

Department of Chemistry, 315 S. 1400 East, University of Utah, Salt Lake City, Utah
84112-0850

Abstract

The hydrostatic pressure dependence of the magnetic ordering temperature, $T_c(P)$, for the interpenetrating, diamondoid lattice-structured, weak ferromagnet (= canted antiferromagnet) $\text{Li}^+[\text{TCNE}]^-$ (TCNE = tetracyanoethylene) reversibly increases from 20.9 to 23.4 K at 9.73 kbar, an increase of 12% with a rate of increase, dT_c/dP , of 0.27 K/kbar. The 5-T magnetization increased by 672% from 186 emuOe/mol at ambient pressure to an average of 1440 emuOe/mol upon application of pressure. The remanent magnetization initially increases 30% from 10.8 to 14.0 emuOe/mol from ambient to 0.06 kbar, and increases further by 6% to a maximum of 14.8 emuOe/mol at 0.56 kbar before declining by 22% to 11.5 emuOe/mol at 9.73 kbar. The pressure-dependent coercive field, $H_{cr}(P)$, initially decreases by 42% from 31.1 Oe at ambient pressure to 18 Oe at 0.06 kbar, then increases to 52 Oe at 9.73 kbar. The canting angle, α , increases by 28% from 0.52° to 0.66° at 0.06 kbar, then decreases by 23% to 0.51° at 9.73 kbar, as well as increases by 2% from 0.536° to 0.548° from 1.8 to 2.5 K, before decreasing by 79% to 0.117° at 19 K. The interlattice interactions are attributed to be the primary exchange mechanism. Thus, $\alpha(T)$ and $\alpha(P)$ have similar dependencies that are attributed to a competition between an increase and a decrease in the intra- and interlayer C•••N interlattice separations as the temperature and pressure increases.

Introduction

$\text{Li}^+[\text{TCNE}]^-$ (TCNE = tetracyanoethylene, C_6N_4) is an organic-based magnet¹ that orders at 21.0 K (T_c) as a weak ferromagnet (= canted antiferromagnet) with a 30-Oe coercivity, 10-emuOe/mol remanent magnetization, and a 0.5° canting angle, α , at 5 K.² The complex structure consists of two interpenetrating PtS type diamondoid structural sublattices depicted in blue and red in Figure 1 that possesses $[\text{TCNE}]^- S = 1/2$ spins in two layers of parallel $[\text{TCNE}]^-$ s that are canted with respect to each other by $\sim 60^\circ$. The closest $[\text{TCNE}]^- \cdots [\text{TCNE}]^-$ separations for the parallel $[\text{TCNE}]^-$ s are the C \cdots N interlattice distances of 3.42 and 3.46 Å at 16 K. $\text{Li}[\text{TCNE}]$ has also been hypothesized to be a high voltage battery electrode^{3a} as well as an electride.^{3b} Attempts to make structurally related materials with other alkali salts of $[\text{TCNE}]^-$ were unsuccessful, as diamagnetic π -dimers of $[\text{TCNE}]^-$, $\pi\text{-}[\text{TCNE}]_2^{2-}$, of $\text{A}_2[\text{TCNE}]_2 \cdot z\text{Solvent}$ (A = Na, K, Rb, Cs) composition exhibiting long, ~ 2.9 Å, $2e^-/4c$ bonds were isolated.^{4,5,6}

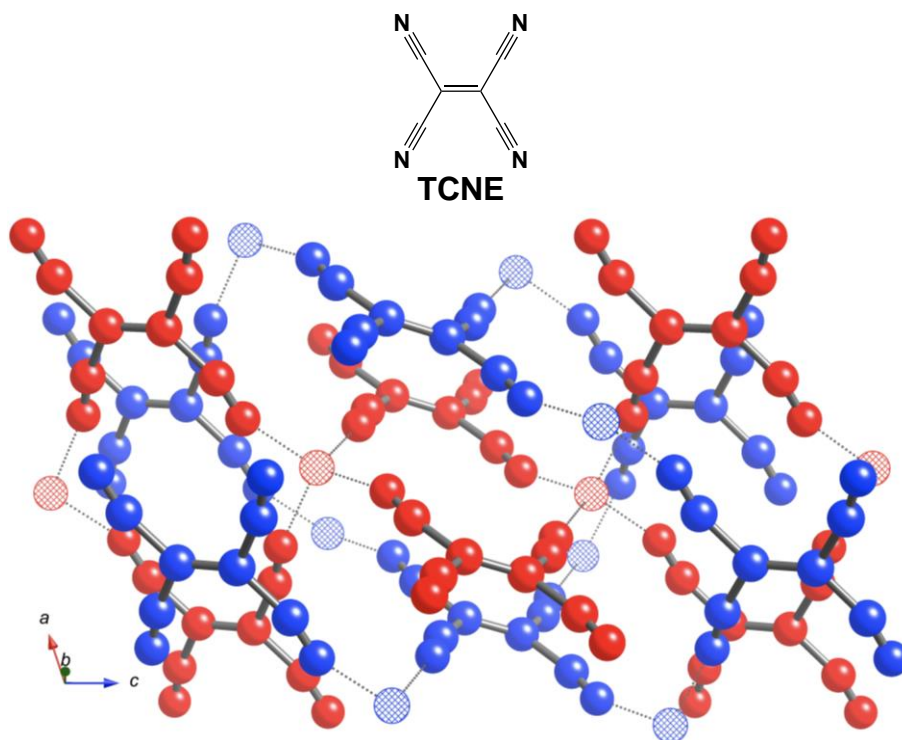


Figure 1. Segment of the $\text{Li}[\text{TCNE}]$ structure almost normal to the ac plane depicting the planar $\mu_4\text{-}[\text{TCNE}]^-$ bound to four tetrahedral Li^+ ions (hatched) with two interpenetrating PtS diamondoid 3-D extended network lattices (red and blue) and layers in the ab and ac planes possessing $[\text{TCNE}]^-$ s whose mean planes are canted by $\sim 60^\circ$ with respect to each other.²

Li[TCNE] consists of only first-row elements, and its T_c exceeds all previously reported organic-based magnets solely comprised of main group elements, e.g. ferromagnetic 4-nitrophenyl nitronyl nitroxide, NPNN ($T_c = 0.6$ K),⁷ weak ferromagnetic 1,3,5-triphenyl-6-oxoverdazyl ($T_c = 5.5$ K),⁸ ferromagnetic 1,3,5,7-tetramethyl-2,6-*N,N*-dioxylidiazadamantanedioxyl ($T_c = 1.48$ K),⁹ and [TDAE][C₆₀] [TDAE = tetrakis(dimethyl-amino)ethylene] ($T_c = 16.1$ K),¹⁰ which is best described as a spin glass.¹¹ An exception is the weak ferromagnet 4'-cyanotetrafluorophenyldithiadiazolyl ($T_c = 35.5$ K).¹² Under hydrostatic pressure the $T_c(P)$ for organic-based magnets solely comprised of main group elements,¹³ e.g. NPNN,^{7, 14} 1,3,5,7-tetramethyl-2,6-*N,N*-dioxylidiazadamantanedioxyl,¹⁵ and [TDAE][C₆₀]¹⁶ decreases, whereas the $T_c(P)$ increases for 4'-cyanotetrafluoro-phenyldithiadiazolyl to 64.4 K at 16 kbar¹⁷ and 1,3,5-triphenyl-6-oxoverdazyl increases at a rate of 0.86 K/kbar up to 10.9 kbar.⁸ The coercivity of Li[TCNE] is unexpectedly higher than that for all other organic-based magnets, except those that are Se-based, due to its greater spin orbit coupling.¹⁸

The weak ferromagnetism for Li[TCNE] suggest a non-compensated two-sublattice antiferromagnet, with spins on two magnetic layers of parallel [TCNE]⁻s along *b* and *c* (Figure 1) that are canted with respect to each other by $\sim 60^\circ$.² Albeit, offset the planar [TCNE]⁻s from the two interpenetrating lattices are separated by 3.120, 3.145, and 3.150 Å at 16, 20 and 50 K, respectively. To further understand the magnetic interactions to greater extent, herein the pressure dependence of the zero-field cooled, M_{ZFC} , field-cooled, M_{FC} , and remanent, M_R , magnetizations are reported. The $M_R(P, T)$ data enables the determination of the canting angle, α , as a function of pressure and temperature, $\alpha(P, T)$, for the first time for any weak ferromagnet.

Experimental Section

Li[TCNE] was prepared as previously described,² and all sample preparations were performed under dry N₂ atmosphere in Vacuum Atmosphere DriLab (<1 ppm O₂). Infrared spectroscopy and magnetic susceptibility were in accord with literature values. A Quantum Design (QD) Superconducting Quantum Interference Device (SQUID) Magnetic Property Measurement System (MPMS 5T; sensitivity = 10⁻⁸ emu or 10⁻¹²

emu/Oe at 1 T) with a low field option was used to perform the low field and pressure dependent measurements as previously described.^{19,20} Magnetic susceptibility data was collected from powder samples loaded into gelatin capsules. Pressure dependence magnetic data were collected in a Kyowa Seisakusho based Be–Cu hydrostatic pressure cell design with zirconia pistons and rubber o-rings. The diamagnetic correction of the powder sample of -64.2×10^{-6} emu/mol was used for the gelatin sample. Magnetic contribution to the pressure cell was measured and subsequently subtracted from the data collected for the pressure cell sample.

To prepare the hydrostatic pressure samples ~1 mg was loaded into a Teflon™ cell with ~3 mg of Sn (Mallinckrodt, 99.9769%) and ~2 mg of decalin in a N₂ atmosphere drybox (<1 ppm O₂) and capped with Teflon plugs. The Sn was used to determine the hydrostatic pressure in situ by observation of its superconducting critical temperature ($T_{sc} = 3.732$ K).²¹ A Kyowa Seisakusho CR-PSC-KY05-1 apparatus performed application of pressure on the cell assembly. The pressure was monitored with a WG-KY03-3 pressure sensor, and an Aikoh Engineering Model-0218B digital sensor readout.

The temperature dependent magnetic measurement data for the zero-field cooled, $M_{ZFC}(T)$, was obtained upon cooling in a zero applied field to 5 K and collected upon warming in a 5 Oe field. The sample was cooled in a 5 Oe field and the data were collected in a 5 Oe field for the field cooled magnetization, $M_{FC}(T)$. After cooling again in a 5 Oe field, data were collected with no applied field for the remanent magnetization, $M_R(T)$. The rates that the temperature was increased were 0.4, 0.1, 0.02, 0.1, and 0.4 K/min for 5-15, 15-18, 18-22, 22-30, and 32-40 K, respectively, for the $M(T)$ data. The data for isothermal field-dependent measurements were collected at 5 K in the persistent field charge mode between 0-100, 100-200, 200-1000, 1000-5000, and 5000-50,000 Oe at 5, 10, 50, 1000, and 5000 Oe increments, respectively. All pressure dependence data were compared to initial gelatin capsule-based data that was collected. The T_c was determined from $M_R(T)$ by extrapolation of the linear most portion of the data to the temperature intercept. Upon reduction from ± 5 T, extrapolation to zero applied field determined the coercive field, H_{cr} , while extrapolation to the magnetization intercept determined the remanent magnetization, $M_R(H)$.

Results and Discussion

At ambient pressure, Li[TCNE] magnetically orders as a weak ferromagnet (canted antiferromagnet; canting angle, $\alpha = 0.5^\circ$) below 21.0 ± 0.1 K, from the bifurcation temperature, T_b , of the field cooled, $M_{ZFC}(T)$, and zero field, $M_{FC}(T)$, cooled magnetizations as well as the temperature at which the remanent magnetization vanishes, $M_R(T) \rightarrow 0$.² Related TCNE-based organic-based magnets exhibit an increase in T_c with increasing pressure, Table 1. For example, the T_c of [FeCp*₂][TCNE] possessing ionic (0-D) [TCNE]⁻ increases from 4.8 to 7.48 K at an average rate of 0.20 K/kbar,^{22,23} while the T_c of 3-D structured Mn^{II}(TCNE)_{3/2}(I₃)_{1/2} possessing μ_4 -[TCNE]⁻ increases from 171 to 273 K at an average rate of 7.18 K/kbar.²⁴

Table 1. Summary of the $T_c(P)$ for n-D (n = 0, 1, 2, 3) network-structured μ_x -[TCNE]⁻-based magnets.

	n-D	x	^a	T_c , ^b K	$T_c(P)$, K (P, kbar)	$\% \Delta T_c / T_c^b$ (ambient)	Ave d T_c/dP , K/kbar	ref
[FeCp* ₂][TCNE]	0-D	0	FO	4.8	7.48 (12.2)	56	0.20	22,23
[Mn ^{III} TCIPP][TCNE]	1-D	2	FI	5.4	8.1 (7.51)	50	0.36	20
Mn ^{II} (TCNE)I(OH ₂)	2-D	4	FI	169	257 (14.05)	52	6.25	24
[Mn ^{II} (TCNE)(NCMe) ₂][SbF ₆]	2-D	4	FI	75	84 (10.1)	12	0.88	25
Mn ^{II} (TCNE) _{3/2} (I ₃) _{1/2}	3-D	4	FI	171	273 (14.32)	60	7.18	24
Mn ^{II} (TCNE)(C ₄ (CN) ₈) _{1/2}	3-D	4	AF	69	97 (12.6)	41	5.75	26
Li[TCNE]	3-D	4	CW	20.9	23.4 (9.73)	12	0.27	This Work

^a Magnetic ordering: FO = ferromagnet; FI = ferrimagnet, AF = antiferromagnet; CW = weak ferromagnet = canted antiferromagnet ^b ambient pressure

The ambient pressure magnetic data of Li[TCNE] were measured at 5 K for comparison to the reported data prior to the study of the pressure dependence. The T_c and T_b were previously determined to be 20.9 and 21.1 K, from the $M_R(T)$ and the bifurcation of the $M_{ZFC}(T)$ and $M_{FC}(T)$ data, respectively.² The ambient pressure H_{cr} and M_R were 31.1 Oe, and 10.8 emuOe/mol in accord with the previously reported values of 30 Oe and 10 emuOe/mol, respectively, but again the saturation at 9 T was not reached authenticating the sample.

The $M_{ZFC}(T,P)$, $M_{FC}(T,P)$, and $M_R(T,P)$ are altered upon the application of pressure, Figure 2. The bifurcation temperature, T_b , of the $M_{ZFC}(T,P)$ and $M_{FC}(T,P)$ data increases monotonically by 18% to 25 K at 9.73 kbar. The T_c determined from the onset temperature of the remanent magnetization, $M_R(T,P) \rightarrow 0$, increases by 12% at a rate of 0.27 K/kbar to 23.4 K at 9.73 kbar, Figures 2b and 3. This linear increase can be

modeled to $T_c(P) = 0.269 \cdot P + 20.94$ K (Figure 3) with the pressure being in units of kbar. The pressure dependence is reversible, as upon the release of the pressure T_c is 21.4 K in accord with the initial value.

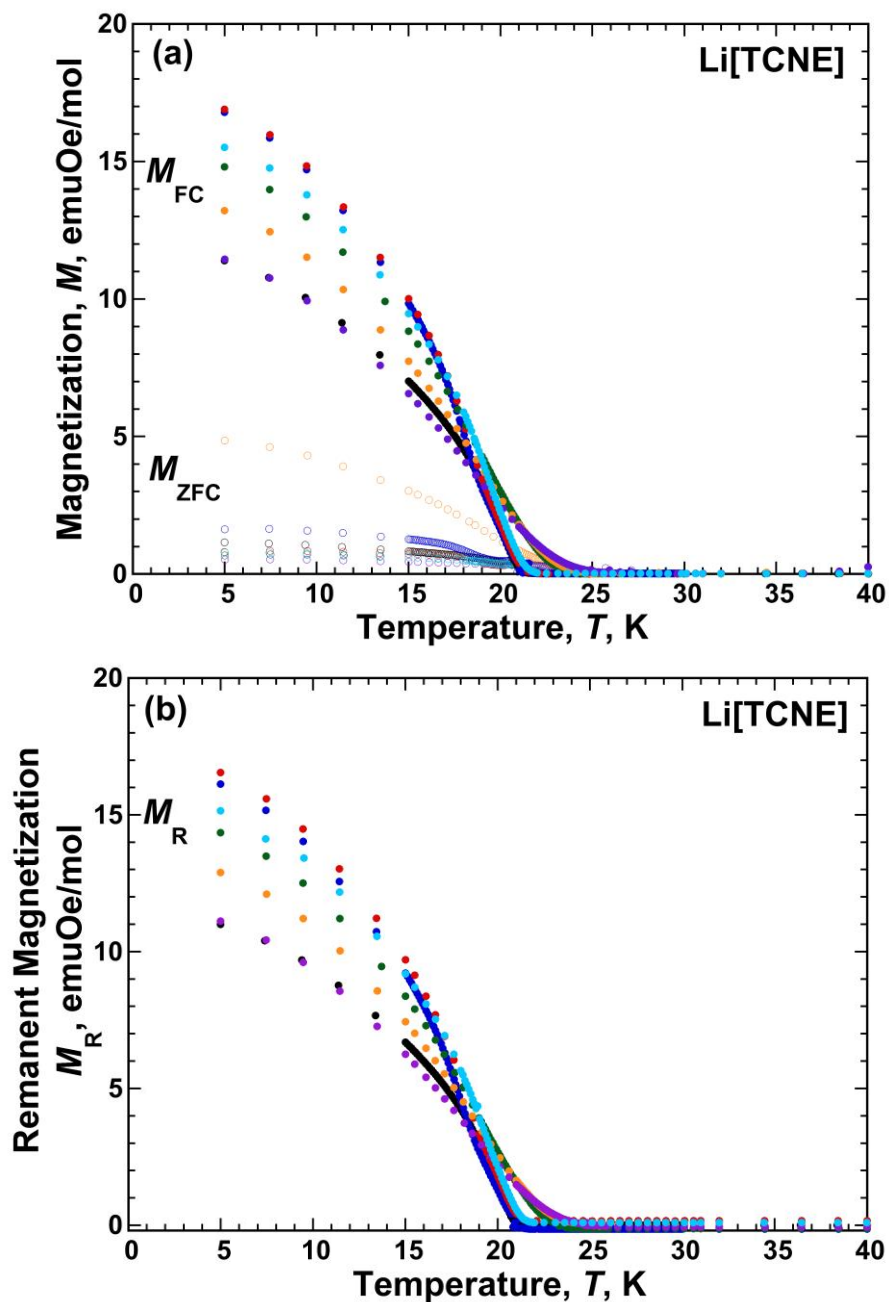


Figure 2. Pressure dependence for Li[TCNE] of the $M_{ZFC}(T)$ (open circles) and $M_{FC}(T)$ (filled circles): 0.001 (black ○●), 0.05 (blue ○●), 0.56 (red ○●), 4.54 (green ○●), 7.56 (orange ○●), 9.73 (purple ○●) kbar, and release of the applied pressure (0.65 kbar; cyan ○●) (a), and $M_R(T)$: 0.001 (black ●), 0.05 (blue ●), 0.56 (red ●), 4.54 (green ●), 7.56 (orange ●), 9.73 (purple ●) kbar and release of the applied pressure (0.65 kbar; cyan ●) (b).

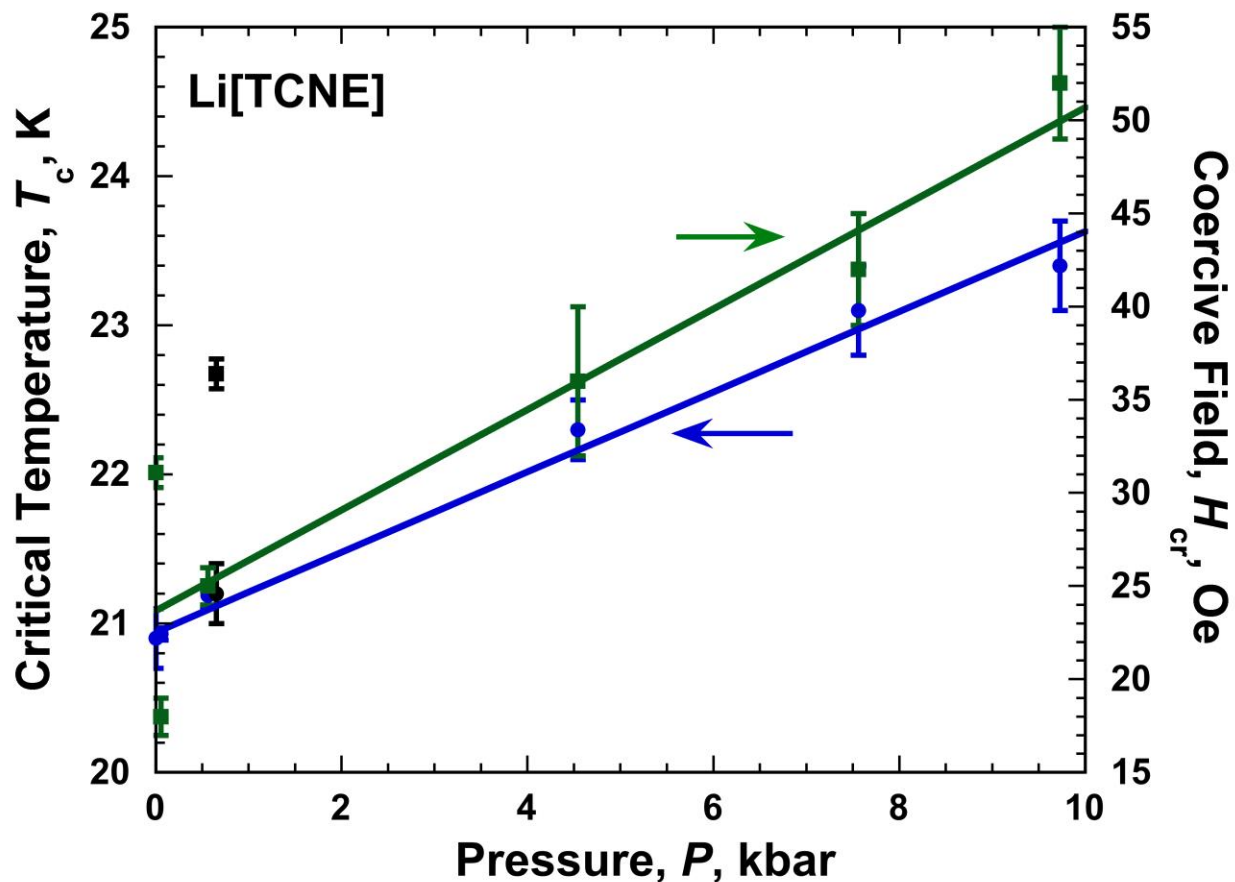


Figure 3. $T_c(P)$ (blue, \bullet) and $H_{cr}(P)$ (green, \square) for Li[TCNE]; the black points are for the released pressure. The equations for the lines modeling the $T_c(P)$ and $H_{cr}(P)$ data are $0.269 \cdot P + 20.94$ K and $2.70 \cdot P + 23.7$ Oe, respectively.

The hysteresis, $M(H)$, was measured at 5 K and $H_{cr} = 31$ Oe at ambient pressure in accord with the previous data.² Since Li[TCNE] is a weak ferromagnet it does not saturate at 5 T with the 5-T magnetization and M_R of 186 and 10.8 emuOe/mol, respectively. In accord with weak ferromagnetic behavior, the saturation magnetization is not achieved at 50 kOe, however the 5 T magnetization increases by $672 \pm 19\%$ from 186 to an average of 1440 ± 40 emuOe/mol for all applied pressures. Upon application of pressure $H_{cr}(P)$ decreased by 42% to 18 Oe at 0.06 kbar, then increased by 189% at an average rate of 2.70 Oe/kbar to 52 Oe at 9.73 kbar, Figure 4. The average linear increase of $H_{cr}(P)$ can be best modeled by $H_{cr}(P) = 2.70 \cdot P + 23.7$ Oe (Figure 3). Likewise, $M_R(P)$ increases by 30% from 10.8 ± 0.1 to 14.0 ± 0.5 emuOe/mol to a maximum of 14.77 ± 0.08 emuOe/mol at 0.56 kbar before decreasing by 22% to 11.5

± 0.04 emuOe/mol at 9.73 kbar, Figure 5. Upon the release of the pressure, $H_{cr}(P)$ returned to 36 ± 4 Oe, and the 5-T and remanent magnetizations returned to 1576.0 ± 0.7 and 13.00 ± 0.08 emuOe/mol, respectively.

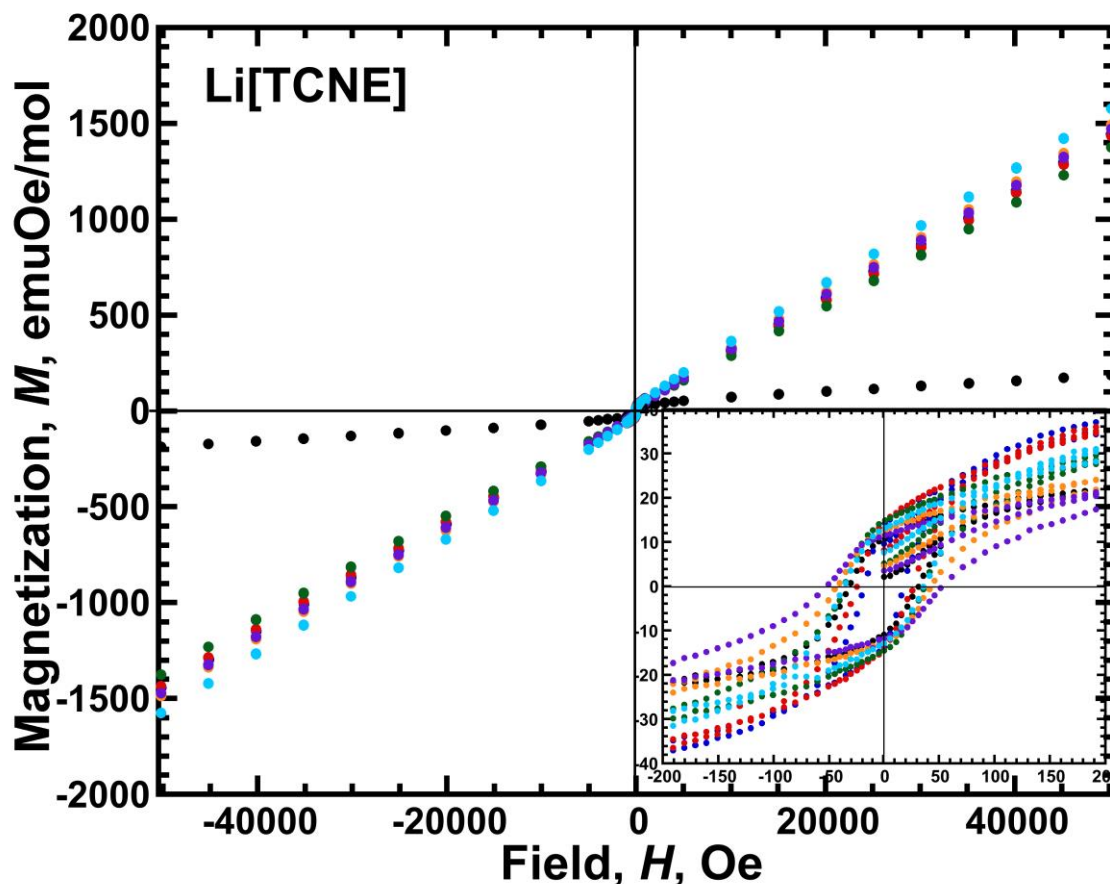


Figure 4. Pressure dependence for Li[TCNE] of the $M(H)$: 0.001 (black ●), 0.05 (blue ●), 0.56 (red ●), 4.54 (green ●), 7.56 (orange ●), 9.73 kbar (purple ●), and release of the applied pressure (0.65 kbar; cyan ●).

Note that the pressure release leads to a field dependent irreversibility, e.g. in the remanent magnetization and coercive field, while the pressure release does not alter T_c .^{27,28} T_c is strongly related to the exchange coupling energy that is expected to increase with increasing pressure due to the decreasing distances between the spin sites. In contrast, the field dependent measurements are more complex depending on more factors, such as intra- and interlayer interactions²⁸ or a metastable state.²⁹ As magnetic saturation is not always achieved, high field magnetization is also not always

reversible^{26,27,28} Formation or presence of defects are also factors that influence the macroscopic field dependent magnetization, and qualitative reversible magnetization can be observed, albeit with changing values and shapes.²⁶ Furthermore, the stress caused by pressurization is not perfectly restored, as it is often easy enough to get 0.5 kbar of pressure just with gentle hand tightening in the initial assembly of the pressure cell apparatus. Decompression of the sample cell is important for reversibility, and is observed at times, however, it is dependent on the stress induced in the pressure cell as well as the behavior of the system under pressure.²⁹ Due to the complex behavior of Li[TCNE] with the rotation and structural changes causing the canting angle to change, it is expected that field dependent measurements would result in a possible metastable condition.

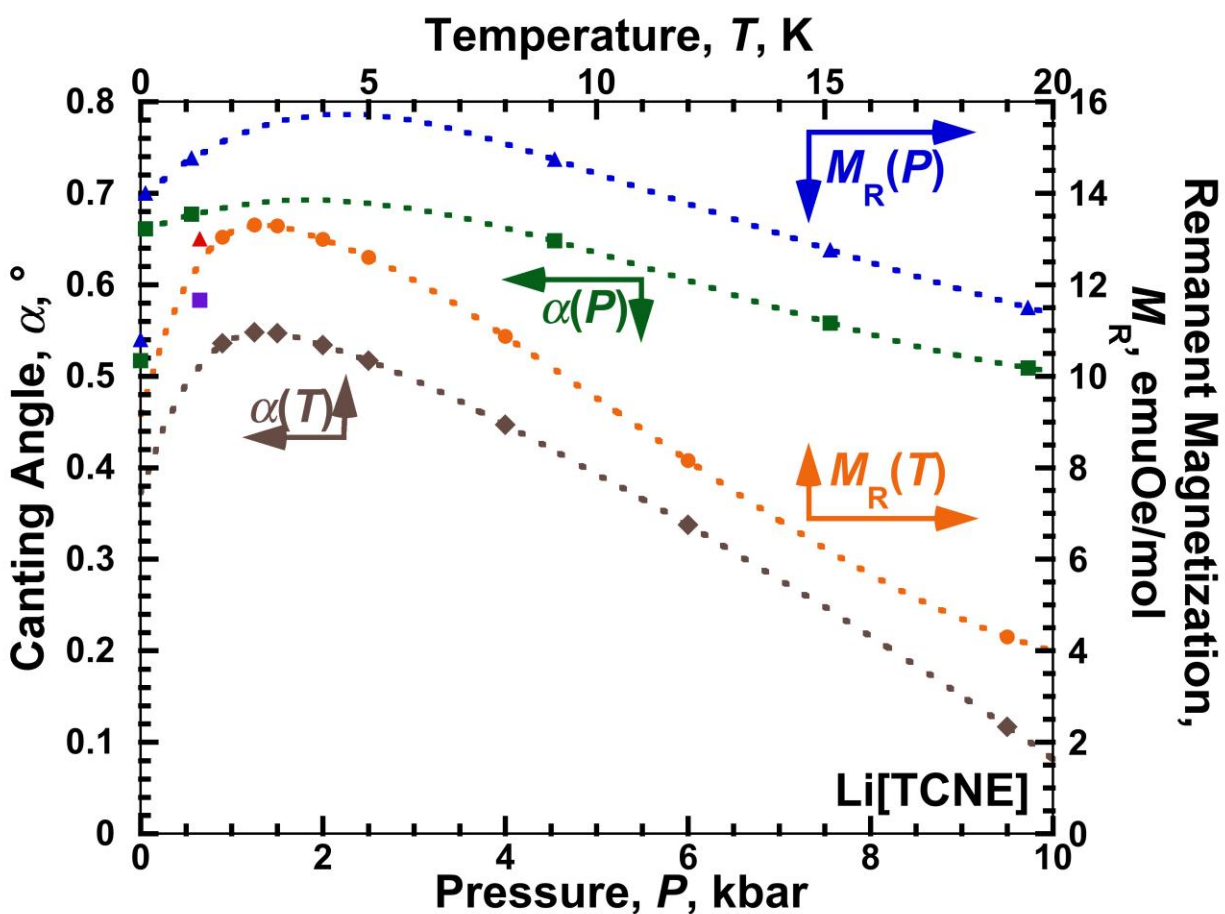


Figure 5. Ambient pressure $\alpha(T)$ (brown \blacklozenge) and $M_R(T)$ (orange \bullet), and 5-K $\alpha(P)$ (green \square) and $M_R(P)$ (blue \blacktriangle) for Li[TCNE]; the red and purple points are for the released pressure for $M_R(P)$ and $\alpha(P)$, respectively. The lines are guides for the eye.

As Li[TCNE] is a weak ferromagnet, the $M_R(T,P)$ was used to determine the canting angle, α , upon application of pressure. At ambient pressure, $\alpha = 0.52 \pm 0.01^\circ$ [from $\sin(\alpha/2) = 2M_R/M_{\text{sat}}^{30}$ ($M_{\text{sat}} = 5585 \text{ emuOe/mol}$)] in accord with previous data.² Near ambient pressure, α increased by 28% to $0.66 \pm 0.02^\circ$ at 0.06 kbar (Figure 5). Further increasing the pressure, however, led to α decreasing by 23% to $0.509 \pm 0.008^\circ$ at 9.73 kbar. Upon release of pressure, α was $0.58 \pm 0.01^\circ$, a 13% increase from ambient pressure, and a decrease of 14% for an expected α of 0.68° for 0.65 kbar. The temperature dependence on the $\alpha(T)$ was also determined to be $0.536 \pm 0.008^\circ$ at 1.8 K that increased by 2% to $0.548 \pm 0.007^\circ$ at 2.5 K before decreasing by 79% to $0.117 \pm 0.002^\circ$ at 19 K (Figure 5); hence, both $\alpha(P)$ and $\alpha(T)$ are similar and reflect $M_R(T,P)$ having a maximum.

To understand the unexpected $\alpha(T)$, the temperature dependent structures at 16, 20 and 50 K² were examined and exhibit temperature dependent atomic separations that correlate with $\alpha(T)$. Within the same set of layers comprised of [TCNE]⁻s from the interpenetrating lattices, Figures 1 and 6a, the interlattice intralayer C \cdots N [TCNE]⁻ \cdots [TCNE]⁻ distances (pink in Figure 6) slightly increases from 3.417 to 3.456 Å as the temperature increases from 16 to 20 K. The interlattice intralayer C \cdots N [TCNE]⁻ \cdots [TCNE]⁻ separation (green in Figure 6) remains constant at 3.460 ± 0.002 Å. However, the interlattice interlayer C \cdots N [TCNE]⁻ \cdots [TCNE]⁻ distance (orange in Figure 6b) slightly decreases from 3.509 to 3.466 Å as the temperature increases from 16 to 20 K. Each of these distances are in the range associated with van der Waals interactions,^{31, 32} and exceed the reported for the weak ferromagnet 4'-cyanotetrafluorophenyldithiadiazolyl with an intermolecular distance of 2.986 Å and a 0.085° canting angle.¹² The intra- and interlayers also exhibit a temperature dependent rotation of [TCNE]⁻ and the decrease and increase in the intra- and interlayer distances (pink and orange in Figure 6b) around the axis formed from the rigid intralayer separation (green Figure 6). These changes in distances as a function of temperature lead to an increase in the angle between the [TCNE]⁻ planes of the adjacent chains for 59.2° at 16 K to 60.5° at 20 K and a decrease in the twist of the [TCNE]⁻ planes of the adjacent chains from 64.0° at 16 K to 61.4° at 20 K. As the temperature increased to 50

K, each of these three distances are 3.467 ± 0.006 Å. A movie showing the interlattice inter- and intralayer $C \cdots N$ [TCNE] $^{-}$ \cdots [TCNE] $^{-}$ distances using the same color code used for Figure 6 is available a Figure S1 in the SI.

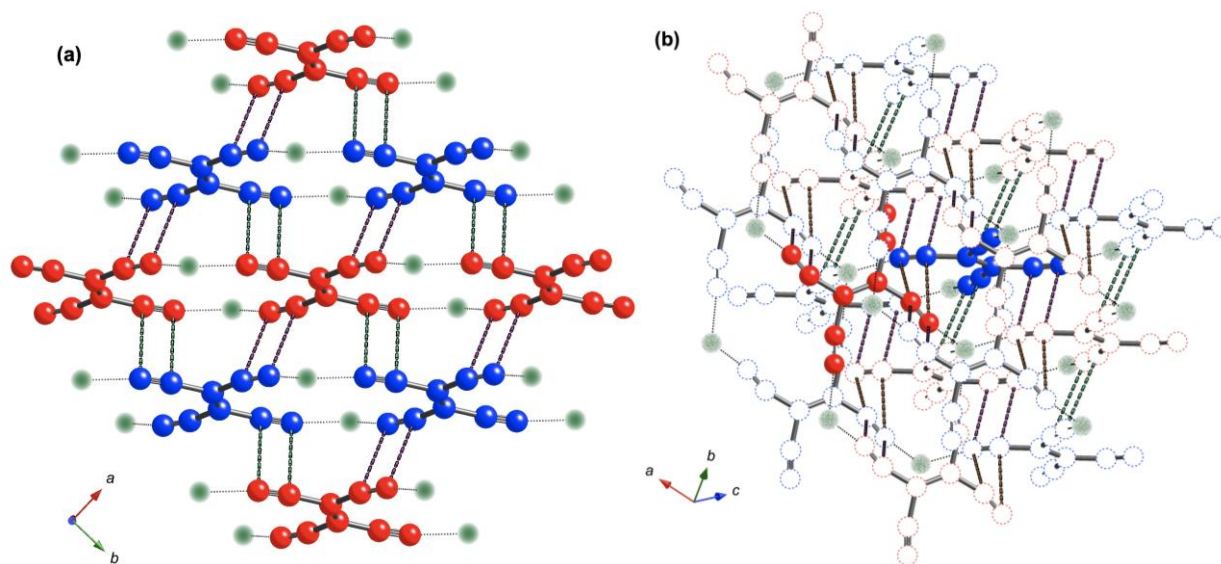


Figure 6. Portion of the Li[TCNE] structure depicting the intra- (a) and interlayer (b) interlattice $C \cdots N$ [TCNE] $^{-}$ \cdots [TCNE] $^{-}$ interactions (Li^{+} is green). The pink and green intralayer $C \cdots N$ [TCNE] $^{-}$ \cdots [TCNE] $^{-}$ interlattice separations are 3.417 and 3.456 Å and 3.458 and 3.462 Å at 16 and 20 K, respectively, and the orange interlayer $C \cdots N$ [TCNE] $^{-}$ \cdots [TCNE] $^{-}$ interlattice separations are 3.509 and 3.466 Å at 16 and 20 K, respectively. The mean interlayer [TCNE] $^{-}$ s planes have 59.2° and 60.5° angles at 16 and 20 K, respectively.

These changes in distances are a consequence of the two different $\angle N-Li-N$ s; one decreasing from 98.50° to 95.80° and the other increasing from 121.37° to 125.56° as the temperature increases from 16 to 20 K. Hence, the bonding about Li^{+} is a distorted tetrahedron. While not understood in detail the competition between the decreasing interlayer and increasing intralayer $C \cdots N$ interlattice [TCNE] $^{-}$ \cdots [TCNE] $^{-}$ distances as well as the change in orientation and twist angles between adjacent planes of [TCNE] $^{-}$ are attributed to the initially increasing and then decreasing values of $\alpha(T)$. A detailed computational analysis evaluating these nearest neighbor spin couplings is in progress.

Conclusion

The application of a hydrostatic pressure to $\text{Li}^+[\text{TCNE}]^-$ leads to a modest, reversible 12% linear increase in the T_c from 20.9 ± 0.2 to 23.4 ± 0.3 K at 9.73 kbar with an average rate of 0.27 K/kbar indicative of an increase in the coupling between the $S = 1/2$ $[\text{TCNE}]^-$ sites. This increase in $T_c(P)$ is in accord with all previous reduced TCNE organic-based magnets (Table 1). All previous reduced TCNE organic-based magnets, however, have direct spin coupling between the $S = 1/2$ $[\text{TCNE}]^-$ and an $S \geq 1$ transition metal ion-based spin-site, which is not present for $\text{Li}[\text{TCNE}]$. In contrast, for several organic based magnets solely comprised of first-row elements, like $\text{Li}[\text{TCNE}]$, e.g. NPNN ,^{7,14} 1,3,5,7-tetramethyl-2,6-*N,N*-dioxylidiazadamantanedioxy,¹⁵ and $[\text{TDAE}][\text{C}_{60}]$,¹⁶ dT_c/dP decreases. The decrease for $[\text{TDAE}][\text{C}_{60}]$ was attributed to itinerant electrons developing. The dT_c/dP for $\text{Li}[\text{TCNE}]$ is comparable to that reported for $[\text{FeCp}^*_2][\text{TCNE}]$ ²³ and $[\text{Mn}^{\text{III}}\text{TCIPP}][\text{TCNE}]$ ²⁰ with average rates of 0.20 and 0.36 K/kbar, respectively. This is attributed to decreasing the separation among the spin centers leading to an increase in the intra- and Interchain interactions. However, the dT_c/dP for $\text{Li}[\text{TCNE}]$ is reduced from 0.88 K/kbar for $[\text{Mn}^{\text{II}}(\text{TCNE})(\text{NCMe})_2][\text{SbF}_6]$ that is strongly correlated to the $[\text{TCNE}]^-$ bond distance decreasing.²⁵ Furthermore, the dT_c/dP is lower 6.25, 7.18, and 5.75 K/kbar, reported for $\text{Mn}^{\text{II}}(\text{TCNE})\text{I}(\text{OH}_2)$, $\text{Mn}^{\text{II}}(\text{TCNE})_{3/2}(\text{I}_3)_{1/2}$, and $\text{Mn}^{\text{II}}(\text{TCNE})(\text{C}_4(\text{CN})_8)_{1/2}$, respectively, due a more complex behavior.^{24,26} Therefore, it is expected that a decrease in the distance between $[\text{TCNE}]^- \cdots [\text{TCNE}]^-$ results in stronger coupling increasing T_c that is observed.

The $H_{\text{cr}}(P)$ initially decreases by 42% from 31 to 18 Oe at 0.06 kbar, prior to subsequently increasing to 52 Oe at 9.73 kbar. The $M_{\text{R}}(P)$ increases to a maximum of 14.77 emuOe/mol at 0.6 kbar, before decreasing by 22% to 11.5 emuOe/mol at 9.73 kbar. Surprisingly, the 5-T magnetization increases 672% increase from 186 emuOe/mol to an average of 1440 ± 40 emuOe/mol.

As a consequence of $M_{\text{R}}(P)$ having a maximum, as is also observed for $M_{\text{R}}(T)$, the canting angle, α , is pressure dependent increasing from $0.52 \pm 0.01^\circ$ at ambient pressure to $0.66 \pm 0.02^\circ$ at 0.06 kbar, before decreasing 23% to $0.509 \pm 0.008^\circ$ at 9.73 kbar. Likewise, $M_{\text{R}}(T)$ increases from $0.536 \pm 0.008^\circ$ at 1.8 K to $0.548 \pm 0.007^\circ$ at 2.5 K, before decreasing 79% to $0.117 \pm 0.002^\circ$ at 19 K; thus, α is also temperature

dependent. The temperature and the pressure dependences show similar properties with a maximum and subsequent decrease, Figure 5, suggests a likely response in the interactions causing the canting angle.

The magnetic anisotropy necessary for weak ferromagnetism is limited to dipole-dipole and Dzyaloshinsky-Moriya (D-M) interactions, with the total Hamiltonian, H , expressed as Eqn 1, for organic-based magnets based upon first row elements and $S = 1/2$ quantum spins, as the single ion anisotropy is absent and the spin-orbit coupling is minimal.^{12,17,33} Here J is the nearest neighbor exchange interaction and D is the antisymmetric interaction that results in the weak ferromagnetic behavior and gives rise to the canting angle (α) and S_i and S_j are the spin operators.^{34,35}

$$H = -2JS_i \cdot S_j + D_{i,j} \cdot (S_i \times S_j) \quad (1)$$

The observed change in canting angle indicates changes in the anisotropy, suggesting that the canted phase is not stable, due to an insignificant anisotropic interaction.³⁶ Therefore, if the magnitude of the antisymmetric interaction is constant, as reported for the weak ferromagnet 4'-cyanotetrafluorophenyldithiadiazolyl, an increase in T_c will be accompanied with a decrease in magnetization.¹⁷ For weak anisotropy, an increase in $|D|$ will increase the canting angle that will affect the magnetic properties.^{8,15}

The genesis of the unexpected increase followed by a decrease in $\alpha(T)$ is attributed the competition between the increase of one of the crystallographically unique $\angle N-Li-N$ and decrease of the other of the crystallographically unique $\angle N-Li-N$ as the temperature is increased. This leads to a decrease and increase in the inter- and intralayer C \cdots N interlattice [TCNE] \cdots [TCNE] \cdots distances, respectively, as well as a change in orientation among both inter- and intralayer [TCNE] \cdots s that alters the magnetic couplings and lead to $\alpha(T)$ and consequently $M_R(T)$ initially increasing before decreasing as the temperature is increased. The decrease in the interlattice distance would be expected to increase in the exchange interaction, J , and on the antisymmetric exchange, $|D|$. The observed increase in T_c reflects the increase in the exchange interaction. A lack of inversion center, being necessary for spin canting, also suggests low symmetry.²⁵ The increase in $H_{cr}(P)$ is also consistent with a changing symmetry and exchange interaction.³⁷ As $\alpha(P)$ has a similar dependence, a similar competition

the interlattice C...N separations within and between [TCNE]⁻ layers is expected from the pressure dependent structures. Further computational studies are necessary to elucidate the detailed spin interactions of Li[TCNE].

Supporting Information

A movie showing the interlattice inter- and intralayer C...N [TCNE]⁻...[TCNE]⁻ distances using the same color code used for Figure 6.

Acknowledgement

We acknowledge partial support by the Department of Energy Division of Materials Science (Grant Nos. DE-FG03-93ER45504). We appreciate the helpful discussions with Eric V. Campbell, Dr. Adora Graham, Prof. Joel M. Harris, Dr. Michael W. Manhart, and Prof. Jamie L. Manson. Images of structures were generated using CrystalMaker[®]; CrystalMaker Software Ltd, Oxford, England.

Conflict of interest

The authors declare no conflict of interest.

ORCID

0000-0001-5743-8327 JSM

Keywords: Tetracyanoethylene · extended 3D structures · weak ferromagnet · interpenetration structure · pressure

References

- 1 a) V. I. Ovcharenko and R. Z. Sagdeev, *Russ. Chem. Rev.* **1999**, *68*, 345-363.
b) S. J. Blundell and F. L. Pratt, *J. Phys.: Condens. Matter* **2004**, *16*, R771-R828.
c) J. S. Miller, *Chem. Soc. Rev.* **2011**, *40*, 3266-2396.
d) J. S. Miller and A. J. Epstein, *Angew. Chem. Int. Ed.* **1994**, *33*, 385-415.
e) J. S. Miller, *Chem. Soc. Rev.* **2011**, *40*, 3266-3296.
f) J. S. Miller, *Materials Today*, **2014**, *17*, 224-235.
- 2 J.-H. Her, P. W. Stephens, R. A. Davidson, K. S. Min, J. D. Bagnato, K. van Schooten, C. Boehme and J. S. Miller, *J. Am. Chem. Soc.* **2013**, *135*, 18060-18062.
- 3 a) Y. Chen and S. Manzhos, *Phys. Chem. Chem. Phys.* **2016**, *18*, 8874-8880.
b) N. Salehi, L. Edjlali, E. Vessally, I. Alkorda and M. Es'haghi, *Comp. Theor. Chem.* **2019**, *1149*, 17-23.
- 4 a) H. Bock, C. Nather and K. Ruppert, *Z. Anorg. Allg. Chem.* **1992**, *614*, 109-114.
b) J. Bagnato, A. R. Atif and J. S. Miller, unpublished results.
- 5 a) S. V. Rosokha, B. Lorenz, T. Y. Rosokha and J. K. Kochi, *Polyhed.*, **2009**, *28*, 4136-4140.
b) J. Casado, P. M. Burrezo, F. J. Ramírez, J. T. L. Navarrete, S. H. Lapidus, P. W. Stephens, H.-L. Vo, J. S. Miller, F. Mota, J. J. Novoa, *Angew. Chem. Internat. Ed.* **2013**, *52*, 6421-6425.
- 6 H. Bock and K. Ruppert, *Inorg. Chem.* **1982**, *31*, 5094.
- 7 M. Kinoshita, *Phil. Trans. R. Soc. Lond. (A)* **1999**, *357*, 2855.
- 8 M. Mito, M. Hitaka, T. Kawae, K. Takeda, K. Suzuki and K. Makai, *Mol. Cryst., Liq. Cryst.* **1999**, *334*, 369.
- 9 R. Chiarelli, A. Rassat, Y. Dromzee, Y. Jeannin, M. A. Novak and J. L. Tholence, *Phys. Scrip.* **1993**, *T49*, 706.
- 10 a) P.-M. Allemand, K. C. Khemani, A. Koch, F. Wudl, K. Holczer, S.; Donovan, G. Gruner, J. D. Thompson, *Science*, **1991**, *253*, 301.
b) A. Lappas, K. Prassides, K. Vavekis, D. Arcon, R. Blinc, P. Cevc, A. Amato, R. Feyerherm, F. N. Gygaz and A. Schenck, *Science*, **1995**, *267*, 1799.

-
- c) B. Narymbetov, A. Omerzu, V. V. Kabanov, M. Tokumoto, H. Kobayashi and D. Mihailovic, *Nature*, **2000**, 407, 883.
- d) B. Narymbetov, H. Kobayashi, M. Tokumoto, A. Omerzu and D. Mihailovic, *Chem. Commun.* **1999**, 1511.
- 11 a) D. Mihailovic, D. Arcon, P. Venturini, R. Blinc, A. Omerzu and P. Cevc, *Science*, **1995**, 268, 400.
- b) A. Omerzu, D. Arcon, R. Blinc and D. Mihailovic, in *Magnetism - Molecules to Materials*, J. S. Miller and M. Drillon, Eds., Wiley-VCH, Mannheim, **2001**, 2, 123.
- 12 A. J. Banister, N. Bricklebank, I. Lavender, J. M. Rawson, C. I. Gregory, B. K. Tanner, W. Clegg, M. R. J. Elsewood and F. Palacio, *Angew. Chem. Int. Ed.* **1996**, 35, 2533-2535.
- 13 K. Takeda and M. Mito, in Carbon-based magnetism, T. Makarova, F. Palacio, Eds. Elsevier, 2006, p. 131.
- 14 K. Takeda, K. Konishi, M. Tamura and M. Kinoshita, *Phys. Rev. B*, **1996**, 53, 3374.
- 15 K. Takeda, M. Mito, K. Kinoshita, M. Novak, J. Tholence and A. Rassat, *Polyhed.* **2003**, 22, 2287.
- 16 J. D. Thompson, G. Sparn, F. Diederich, G. Grüner, K. Holczer, R. B. Kaner, R. L. Whetten, P.-M. Allemand, Q. Li and F. Wudl, *Mat. Res. Soc. Symp.* **1992**, 247, 315-320.
- 17 M. Mito, T. Kawae, K. Takeda, S. Takagi, Y. Matsushita, H. Deguchi, J. M. Rawson and F. Palacio, *Polyhed.* **2001**, 20, 1509-1512.
- 18 C. M. Robertson, A. A. Leitch, K. Cvrkalj, R. W. Reed, D. J. T. Myles, P. A. Dube and R. T. Oakley, *J. Am. Chem. Soc.* **2008**, 130, 8414-8425.
- 19 E. J. Brandon, D. K. Rittenberg, A. M. Arifv J. S. Miller, *Inorg. Chem.* **1998**, 37, 3376.
- 20 J. G. DaSilva and J. S. Miller, *Polyhed.* **2013**, 68, 76-79.
- 21 L. D. Jennings and C. A. Swenson, *Phys. Rev.* **1958**, 112, 31.
- 22 Z. J. Huang, F. Cheng, Y. T. Ren, Y. Y. Xue, C. W. Chu and J. S. Miller, *J. Appl. Phys.* **1993**, 73, 6563-6564.

-
- 23 J. G. DaSilva, R. Clérac and J. S. Miller, *Inorg. Chem.* **2013**, *52*, 11677-11683.
- 24 J. G. DaSilva, A. C. McConnell and J. S. Miller, *Inorg. Chem.* **2013**, *54*, 4629-4634.
- 25 A. E. Midgley, C. Olson, C. L. Heth, A. N. Caruso, M. B. Kruger, G. J. Halder, J. A. Schlueter and K. Pokhodnya, *J. Chem. Phys.* **2013**, *138*, 014701.
- 26 A. C. McConnell, J. D. Bell and J. S. Miller, *Inorg. Chem.* **2012**, *51*, 9978-9982.
- 27 T. Tajiri, S. Matsumoto, H. Deguchi, M. Mito, S. Takagi, C. Moriyoshi, K. Itoh, K. Koyama, *J. Magn. Magn. Mat.* **2007**, *310*, e566-e568
- 28 J. G. DaSilva, J. S. Miller, *Inorg. Chem.* **2013**, *52*, 1418–1423.
- 29 E. Coronado, M. C. Gimeñez-López, T. Korzeniak, G. Levchenko, F. M. Romero, A. Segura, V. García-Baonza, J. C. Cezar, F. M. F. de Groot, A. Milner, M. Paz-Pasternak, *J. Am. Chem. Soc.* **2008**, *130*, 15519-15532.
- 30 I. Bhowmick, E. A. Hillard, P. Dechambenoit, C. Coulon, T. D. Harris and R. Clérac, *Chem. Commun.* **2012**, *48*, 9717–9719.
- 31 S. S. Batsanov, *Inorg. Mat.* **2001**, *37*, 1031 – 1046.
- 32 C. Janiak, *J. Chem. Soc., Dalton Trans.*, **2000**, *21*, 3885 – 3896.
- 33 a) C. A. Masmanidis, H. H. Jaffe and R. L. Ellis, *J. Phys. Chem.* **1975**, *79*, 2052–2061.
b) Q. Tian and S. Xie, *Micromachines*, **2019**, *10*, 596-626
c) M. Böchmann, M. Klessinger and M. C. Zerner, *J. Phys. Chem.* **1996**, *100*, 10570–10579
- 34 a) I. Dzyaloshinsky, *J. Phys. Chem. Solids*, **1958**, *4*, 241-255.
b) T. Moriya, *Phys. Rev.* **1960**, *117*, 635-647.
c) T. Moriya, *Phys. Rev.* **1960**, *120* 91-98.
- 35 W. Fujita and K. Awaga, *Mol. Cryst., Liq. Cryst.* **2000**, *341*, 389-393.
- 36 M. Duraj and A. Szytula, *Phys. Stat. Sol. (b)* **2003**, *236*, 470-473.
- 37 a) D. Givord M. F. Rossignol and D. W. Taylor, *J. Phys., IV Proc.*, EDP Sciences, **1992**, *2*, C3-95-104.
b) G. Bertotti, in *Hysteresis in Magnetism*, Academic Press, 1998, p 347-390.